


Title

| |
|--|
| |
|--|

Abstract

[illegible]

If thesis project, name of the student:

| | |
|---|--|
| If thesis project, name of the student: | |
|---|--|

Please list permanent IP
addresses for remote observing:

| |
|--|
| |
| |

12m Requested hours per receiver band:

| | | | | | | | |
|------|--|------|--|------|--|------|--|
| 4mm: | | 3mm: | | 2mm: | | 1mm: | |
|------|--|------|--|------|--|------|--|

Total 12M time request at each LST: List total number of shifts (integers only) at each LST for all receivers added together:

[illegible]

SMT Requested hours per receiver band:

| | | | |
|------|--|--------|--|
| 1mm: | | 0.8mm: | |
|------|--|--------|--|

Total SMT time request at each LST: List total number of shifts (integers only) at each LST **separately for 1mm/0.8mm**

[illegible]

1 Scientific Justification

Large-scale observations of CO and thermal dust continuum emission from molecular clouds indicate that their structure is characterized by filaments and clumps with embedded dense cores (e.g. Goldsmith et al. 2008, André et al. 2014, Hacar et al. 2023). Many fundamental questions still remain about how filaments and cores evolve within their environment. How do starless cores initially fragment and subsequently grow in mass to become bound and collapsing prestellar cores? How does mass flow onto and within filaments and what is the relative importance of turbulence and magnetic fields in mass flow processes? In order to answer these questions, we must study the simultaneous evolution of filaments and starless cores. This can be achieved by probing the physical and kinematic structure from the multi-parsec filamentary scales down to sub-0.1 pc core scales. There is no single, magic tracer that can simultaneously probe all of these scales. In this proposal, we shall map the 2-degree wide central L1495 filaments in Taurus Molecular Cloud using the Arizona Radio Observatory 12m telescope in a complementary set of low to intermediate (HCO^+ , CCH, H_2CO), intermediate to dense (HNC, NO), and dense gas tracers (DNC) that probe different chemistry and different physical structures. This proposal builds on a research education model for large undergraduate group research projects with peer learning that results in student-led papers (i.e. Calahan et al. 2018).

Much of the Taurus Molecular Cloud has been mapped in the inversion transitions of NH_3 using the 100m GBT (Seo et al. 2015, Friesen et al. 2017). NH_3 provides a good probe of the gas kinetic temperature of cold gas ($T_k \leq 30$ K) as well as being a "late-time" chemical tracer of dense molecular gas; however, it is an incomplete tracer of molecular gas in filaments and cores. It is well known that young, potentially transitory, starless cores are not well traced by NH_3 (1,1) emission. For instance, the *Herschel* submillimeter continuum maps of L1495 (Marsh et al. 2016) find over 100 starless cores while the comparable-resolution NH_3 map (Seo et al. 2015) identifies only 39 cores. Another example can be seen with the chemical differentiation between NH_3 and carbon chain molecule emission (Fig. 1). In order to form a complete picture of the physical distribution and kinematics of the intermediate and dense molecular gas, we must use complementary tracers that probe both lower and higher excitation densities than NH_3 (Shirley 2015), as well as earlier and later chemical times than traced by NH_3 alone.

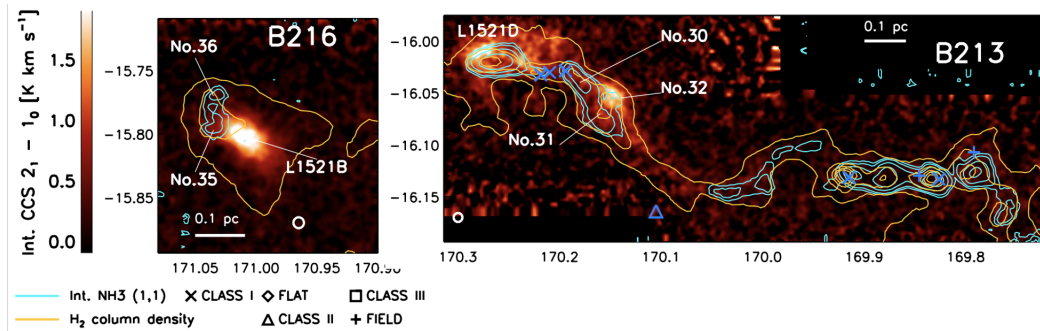


Figure 1: Examples of chemical differentiation in the central L1495 Taurus filaments. The integrated intensity of CCS (underlying image) often does not overlap with the integrated intensity of NH_3 (1,1) (cyan contours) (Seo et al. 2019). 500 μm dust continuum has orange contours.

A goal of this proposal is to constrain how mass flows on to and within filaments. There are three main aspects of the spectra that we shall use to constrain mass flow: maps of the line-of-sight velocity, line width, and the line shape. One of the major challenges to any analysis that attempts to

constrain line centroid, width, and shape is the potential presence of multiple velocity components along the line-of-sight. This problem has recently been solved by the GAS team (of which YS is a member) with the development of a Python multi-component fitting routines for spectral line cubes of transitions with hyperfine structure (e.g., MUFASA; M. Chen et al. 2020). For example, the complicated velocity structure in NH_3 (1,1) of the NGC 1333 region was deconstructed and analyzed to reveal several velocity coherent filaments (Fig. 2). The gradient in v_{LSR} at each pixel may be decomposed into components that are locally parallel and perpendicular to the filament ridge. The map for the parallel components show oscillatory behavior (appearing as zebra stripes across the filaments in Fig. 2) that are not correlated with dense cores within the filaments and are therefore not likely due to periodic gravitational instabilities, but instead are more likely related to turbulent motions or waves predicted in turbulent MHD simulations (i.e. Offner & Liu 2018). The analysis of the perpendicular component shows some regions have a decreasing velocity gradient (unexpected!) toward the filament ridge for several filaments, consistent with a slowing of the gas flow if it interpreted as accretion onto the filaments. The NGC 1333 region is very complicated with feedback from embedded protostars likely affecting the structure and kinematics of the filaments in this region (Plunkett et al. 2013). The L1495 filaments of Taurus have much less protostellar feedback and will provide a critical comparison region.

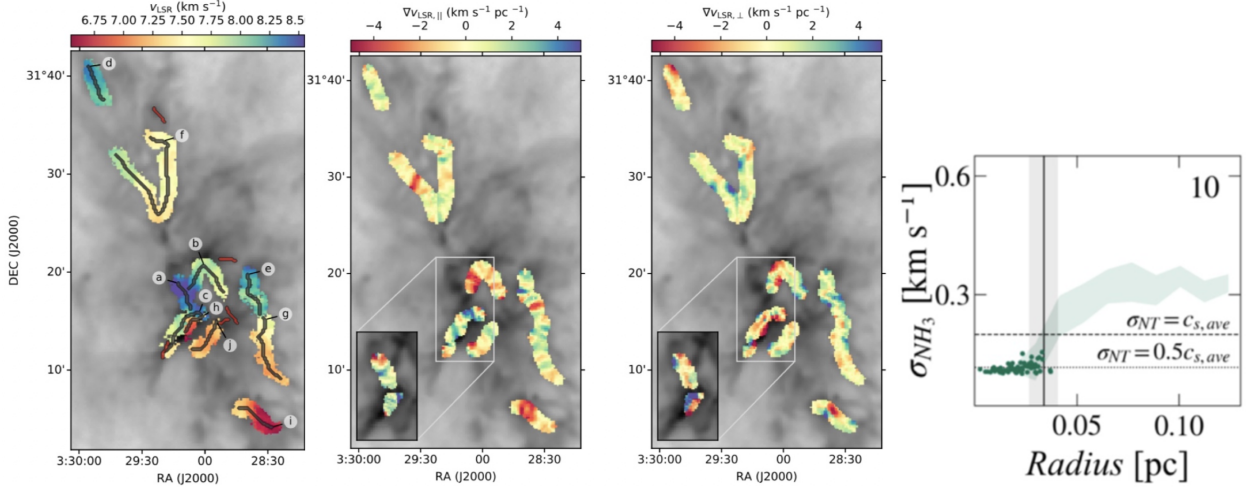


Figure 2: LEFT 3 Panels: The v_{LSR} of coherent structures identified in NH_3 spectra toward NGC 1333 using the Python multi-velocity component fitting tool (Chen et al. 2020). Perpendicular and parallel components of ∇v_{LSR} with respect to the filament spines. NH_3 alone misses structure seen in the underlying dust continuum map; hence the need for other molecular tracers. RIGHT: Example of transition to coherence seen in NH_3 emission toward a core (Chen et al. 2019).

Our survey will probe the line width (both velocity dispersion and Full Width Zero Intensity) with a sub-sonic velocity resolution of 0.07 – 0.12 km/s. The line width is an indicator of the projected line-of-sight motions within the telescope beam while the FWZI may be used to search for non-Gaussian features such as line wings due to protostellar outflows. Our survey will use high spectral resolution observations to map the ratio of thermal to non-thermal line width using probes of varying chemistry and varying densities along each line-of-sight. A transition to coherence (see right panel of Fig. 2) is not obvious in our NH_3 observations of L1495; they are thermally dominated throughout our map (Seo et al. 2015). We shall use our observations to search for this signature in these regions. This is a very important quantity to measure for a stability analysis (i.e. using the Virial Theorem) of both the dense cores and the filaments (see Scibelli et al. 2023).

2 Technical Justification

We propose to map the L1495 filaments in the Taurus Molecular Cloud with 20 observing shifts (23h - 9h LST) with the the 3mm and 2mm MRI sideband separating receivers. The region is covered by 8 OTF maps that are $15' \times 15'$ (Fig. 3) with a scan rate of $15''/\text{s}$ and row spacings of $24''$ at 3mm and $14''$ at 2mm. Based on our prior OTF mapping, we shall observe each OTF map 4 times (2 RAmaps and 2 DECmaps; 2 hours/map for a total of 8 hours) in order to reach a baseline rms of < 0.1 K in the center of the map (similar to the NH_3 baseline rms). 16 shifts are required (one region/shift/receiver), with the exception of B10 where we will go $> 2\times$ deeper at 3mm (4 additional shifts) for a robust comparison of HNC abundance with Hannah Gruber’s pointed dense core chemical survey of that region.

We have selected 8 transitions (one 2-1 and seven ground state) at 3mm and 2mm spanning over 3 orders of magnitude in critical density that probe different physical and chemical environments. All observations will use AROWS Mode 13 (four 40 MHz windows at 19.5 kHz resolution). We shall test the critical densities of each species by comparing their detection statistics with A_V . HCO^+ is an optically-thick intermediate density gas tracer (Shirley 2015) whose line shape may be used as an extended infall tracer by searching for blue-asymmetries when compared with optically thin H^{13}CO^+ (see Gregersen et al. 2000, Reiter et al. 2011, Calahan et al. 2018). HNC is an intermediate to dense gas tracer ($n > \text{few} \times 10^3 \text{ cm}^{-3}$; Pety et al. 2017) that is an abundant isomer to HCN (\sim factor of 2 in abundance) which is popular for extragalactic dense gas studies (i.e. Gao & Solomon 2004). CCH is the simplest hydrocarbon and H_2CO a precursor organic molecular that are ”early-time” chemical tracers (form rapidly compared to NH_3 and deplete in the centers of chemically evolved cores; Spezzano et al. 2017) with low critical densities, probing the interface between cores and filaments. These two molecules are expected to have strong chemical differentiation with organic molecules more abundant in environments shielded from uv radiation and hydrocarbons preferring less shielded radiation fields (see Spezzano et al. 2016, Nagy et al. 2019). NO is thought to be a dense gas tracer, but there is evidence it can deplete at $n > 10^5 \text{ cm}^{-3}$ (Akyilmaz et al. 2007). Finally, DNC, the deuterated isotopologue of HNC, is our densest gas tracer ($n > 10^4 \text{ cm}^{-3}$, Shirley 2015) and chemically later-time tracer than NH_3 . Deuterated-isotopologues fractionate in abundance by several orders in magnitude above the interstellar atomic $[\text{D}]/[\text{H}]$ ratio (Ceccarelli et al. 2014) in cold ($T_d < 10$ K), dense gas. $[\text{DNC}]/[\text{HNC}]$ is a core evolutionary indicator with more chemically evolved cores have higher deuterium fractions that may be used to sort cores into fast and slow dynamical evolution (see Galloway-Spreitsma et al. 2022). Prior 12m observations show that DNC is the brightest deuterated-molecule to map in these regions (Fig. 3).

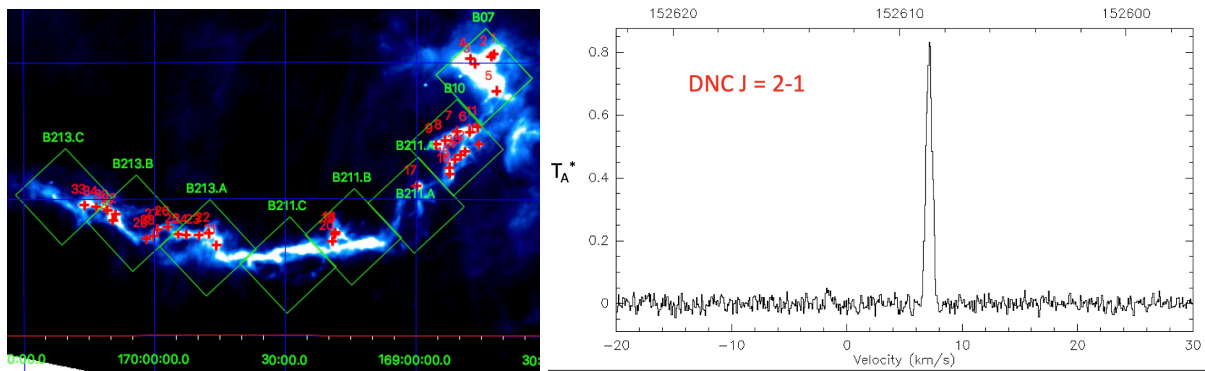


Figure 3: LEFT: OTF Mapping regions for the central L1495 Taurus filaments ($500 \mu\text{m}$ image). Each region is $15'/\text{side}$. RIGHT: DNC 2-1 observed January 2024 for H. Gruber Honors Thesis.

References

- Akyilmaz M., Flower D. R., Hily-Blant P., et al., 2007, A&A, 462, 221
- Ambrose H. E., Shirley Y. L., Scibelli S., 2021, MNRAS, 501, 347
- André, P., Di Francesco, J., Ward-Thompson, D., et al. 2014, PP VI, 27
- Calahan J. K., Shirley Y. L., Svoboda B. E., et al., 2018, ApJ, 862, 63
- Ceccarelli C., Caselli P., Bockelée-Morvan D., et al., 2014, prpl.conf, 859
- Chen H. H.-H., Pineda J. E., Goodman A. A., Burkert A., et al., 2019, ApJ, 877, 93
- Chen M. C.-Y., Di Francesco J., Rosolowsky E., et al., 2020, ApJ, 891, 84
- Friesen R. K., Pineda J. E., co-PIs, Rosolowsky E., et al., 2017, ApJ, 843, 63
- Galloway-Sprietsma M., Shirley Y. L., Di Francesco J., et al., 2022, MNRAS, 515, 5219
- Gao Y., Solomon P. M., 2004, ApJ, 606, 271
- Goldsmith P. F., Heyer M., Narayanan G., et al., 2008, ApJ, 680, 428
- Gregersen E. M., Evans N. J., Mardones D., Myers P. C., 2000, ApJ, 533, 440
- Hacar A., Clark S. E., Heitsch F., et al., 2023, ASPC, 534, 153
- Marsh K. A., Kirk J. M., André P., et al., 2016, MNRAS, 459, 342
- Nagy Z., Spezzano S., Caselli P., et al., 2019, A&A, 630, A136
- Offner S. S. R., Liu Y., 2018, NatAs, 2, 896
- Pety J., Guzmán V. V., Orkisz J. H., et al., 2017, A&A, 599, A98
- Plunkett A. L., Arce H. G., Corder S. A., et al., 2013, ApJ, 774, 22
- Reiter M., Shirley Y. L., Wu J., et al., 2011, ApJ, 740, 40
- Scibelli S., Shirley Y., 2020, ApJ, 891, 73
- Scibelli S., Shirley Y., Vasyunin A., Launhardt R., 2021, MNRAS, 504, 5754
- Scibelli S., Shirley Y., Schmiedeke A., et al., 2023, MNRAS, 521, 4579
- Seo Y. M., Shirley Y. L., Goldsmith P., et al., 2015, ApJ, 805, 185
- Seo Y. M., Majumdar L., Goldsmith P. F., Shirley Y. L., et al., 2019, ApJ, 871, 134
- Shirley Y. L., 2015, PASP, 127, 299
- Spezzano S., Bizzocchi L., Caselli P., et al., 2016, A&A, 592, L11
- Spezzano S., Caselli P., Bizzocchi L., et al., 2017, A&A, 606, A82